CLM-R256



CLM-R256



UKAEA

Report

# TRANSIENT DEBRIS BED CALCULATIONS IN ONE DIMENSION

N. J. BREALEY

CULHAM LABORATORY
Abingdon Oxfordshire
1985
Available from H. M. Stationery Office
Price £4.00

CLM-R 256

# TRANSIENT DEBRIS BED CALCULATIONS IN ONE DIMENSION

N.J.Brealey
Theoretical Physics Division,
Culham Laboratory,
Abingdon,Oxfordshire OX14 3DB,UK.

Abstract

A model for transient heat and mass transfer in internally heated debris beds is described. The model is based on conservation laws for mass and energy with phenomenological laws for flow through a porous medium. A numerical scheme based on an enthalpy method has been developed: the scheme for one dimensional beds has been implemented in the code ENTH. Two example calculations are presented. Some model limitations and possible enhancements of ENTH are discussed.

September 1985

CONTENTS

## 1. INTRODUCTION

The formation of debris beds is postulated in various (highly unlikely) severe accident sequences in liquid cooled fission reactors. These debris beds consist of core material in a fragmented or particulate form surrounded by coolant. Substantial amounts of heat may be generated by the decay of fisson products in the particulate. This internal source of heat may lead to boiling of the coolant which gives rise to two phase flow of coolant liquid and vapour phases. There may be parts of the bed where only one phase is present.

The most successful model for debris bed heat transfer [1] is based on conservation laws for mass and energy with phenomenological laws for flow through a porous medium. This model has been applied previously to 1-D situations of two kinds, viz. (i) steady-state situations with subcooled, boiling and dried-out regions present in the bed [2] and (ii) transient situations with no subcooling up to the onset of dryout (i.e. a fixed boiling region) [3]. This paper describes the development of a numerical scheme for solving the full transient equations with sub-cooled, boiling and dried-out regions present in the bed. This paper also describes the implementation of this numerical scheme for 1-D situations in a new code, ENTH, and the application of this code to the interpretation of experimental data.

A major application of ENTH is the analysis of debris bed experiments which simulate decay heating by various means such as dielectric heating or neutron heating in a reactor ($UO_2$ debris). These experiments provide large amounts of time dependent data which is useful for model development /validation when it is compared with the predictions of the model.

## 2. BED MODEL

The physical model used has been described extensively elsewhere [1], [3]. However, a brief account is presented here.

## 2.1 Model Basis

The model is based on concepts of two phase flow in porous media. The one dimensional model is described. However extension to higher dimensions is mostly straight forward. There are three different types of region in the bed in which different physical processes must be modelled. They are:

i) Subcooled regions: the temperature T in these regions is below the boiling temperature $T_{bp}$ i.e. $T < T_{bp}$. The pore spaces are occupied by liquid.

ii) Boiling regions: $T = T_{bp}$. The pore spaces are occupied by vapour and liquid.

iii) Dried-out regions: $T > T_{bp}$. The pore spaces are occupied by vapour.

A series model is used for the heat transfer between regions. This model assumes that vapour condenses immediately it contacts a subcooled region and that all liquid vaporizes when it contacts a dried-out region. These assumptions imply that a conducted heat flux at the boundary of a single phase region appears as a liquid/vapour flux on the boiling side of the boundary.

The boiling region model includes capillary pressure effects and uses either the Darcy drag law or the Ergun drag law for each phase. These equations omit inertial terms. In single phase regions i) and iii) conduction and advection are the only forms of heat transfer modelled. Mass and energy balances are applied in all regions. The fluid phases and debris are asssumed to be in local thermal equilibrium.

Pressure variations within the bed are assumed to be sufficiently small that the variation of physical properties with pressure can be neglected. Variations of the physical properties with temperature in the bed are also neglected and properties at the boiling point temperature are used. The model does not treat some phenomena such as steel melting, bed disruptions and channelling, and hysteresis in capillary pressure. These points are discussed in section 7.

## 2.2 Conservation Equations

Conservation of mass is described in all regions of the bed by

$$\varepsilon(\rho_\ell - \rho_v)\frac{\partial s}{\partial t} + \frac{\partial}{\partial z}(\rho_v U_v + \rho_\ell U_\ell) = 0 \qquad (2.1)$$

where

s is liquid saturation - the fraction of pore space occupied by liquid

z is bed height

t is time

U is superficial velocity

$\rho$ is density

$\varepsilon$ is porosity (void fraction of bed)

Subscripts $\ell$, v denote liquid and vapour respectively

Heat balance is governed by different equations in each region. It is in the boiling region

$$\varepsilon \frac{\partial s}{\partial t} = \frac{\partial U_v}{\partial z} - \frac{q}{\rho_v L} \qquad (2.2)$$

in the subcooled region

$$\left[(1-\varepsilon)\rho_d c_d + \varepsilon\rho_\ell c_\ell\right]\frac{\partial T}{\partial t} + \frac{\partial}{\partial z}(\rho_\ell(h_\ell^o + c_\ell(T-T_{bp}))U_\ell) = \frac{\partial}{\partial z}(k\frac{\partial T}{\partial z}) + q \qquad (2.3)$$

and in the dried-out region.

$$\left[(1-\varepsilon)\rho_d c_d + \varepsilon\rho_v c_v\right]\frac{\partial T}{\partial t} + \frac{\partial}{\partial z}(\rho_v(h_v^o + c_v(T-T_{bp}))U_v) = \frac{\partial}{\partial z}(k\frac{\partial T}{\partial z}) + q \qquad (2.4)$$

where

q is heating rate

$h_\ell^o$ is specific enthalpy of liquid at $T = T_{bp}$

$h_v^o$ is specific enthalpy of vapour at $T = T_{bp}$

$L = h_v^o - h_\ell^o$ is the latent heat of vaporisation

T is temperature

c is specific heat

k(s) is effective thermal conductivity ($k(s=0)=k_{dry}$, $k(s=1)=k_{sat}$)

subscript bp denotes boiling point.

subscript d denotes debris

## 2.3 Flow Equations

Dynamical equations for the fluid flow are required in addition to the conservation equations for mass and energy.

$$\frac{\rho_v \nu_v}{K\phi_v}\left(1 + \frac{\alpha d \left|U_v\right|}{(1-\varepsilon)\nu_v f_v}\right) U_v = \rho_v g - \frac{\partial p_v}{\partial z} \tag{2.5}$$

$$\frac{\rho_\ell \nu_\ell}{K\phi_\ell}\left(1 + \frac{\alpha d \left|U_\ell\right|}{(1-\varepsilon)\nu_\ell f_\ell}\right) U_\ell = \rho_\ell g - \frac{\partial p_\ell}{\partial z} \tag{2.6}$$

p is pressure in the phase

g is the acceleration due to gravity

K is permeability

$\nu$ is kinematic viscosity

$\phi$ is the relative permeability of the phase

f is the turbulent enhancement of the relative permeability

d is the effective diameter of debris particles including a shape factor

$\alpha$ is a parameter. In this paper $\alpha=0$ or $\alpha=0.01$.

For $\alpha = 0$ these equations reduce to the Darcy drag law, for $\alpha \neq 0$ they are known as the Ergun equations. These equations omit inertial effects.

In the boiling region the liquid and vapour pressure are related through the capillary pressure.

$$p_c = p_v - p_\ell = \sigma \cos\theta \left(\frac{\varepsilon}{K}\right)^{1/2} J(s) \tag{2.7}$$

where

$\sigma$ is the surface tension

$J(s)$ is the dimensionless Leverett function

$\theta$ is the wetting angle

This is combined with the two flow equations (2.5) and (2.6) to give

$$\frac{\rho_v \nu_v}{K\phi_v}\left(1 + \frac{\alpha d \left|U_v\right|}{(1-\varepsilon)\,\nu_v f_v}\right) U_v - \frac{\rho_\ell \nu_\ell}{K\phi_\ell}\left(1 + \frac{\alpha d \left|U_\ell\right|}{(1-\varepsilon)\nu_\ell f_\ell}\right) U_\ell$$

$$= (\rho_\ell - \rho_v)g - \sigma \cos\theta \left(\frac{\varepsilon}{K}\right)^{1/2} \frac{dJ}{ds} \frac{\partial s}{\partial z} \qquad (2.8)$$

In subcooled regions

$$U_v = 0 \qquad (2.9)$$

In dried-out regions

$$U_\ell = 0 \qquad (2.10)$$

The heat flux, mass flux, pressures and temperature are continuous across interfaces between regions. However, their spatial derivatives need not be continuous.

The continuity of capillary pressure implies that saturation is continuous provided $\varepsilon$ and $K$ are continuous.

## 3. BOUNDARY CONDITIONS

Various boundary conditions are used at the top and bottom of the bed.

### 3.1 Top of Bed (at $z = z_{max}$)

#### 3.1.1 Subcooled overlying pool

The conducted heat flux at the top of the bed is related to the surface-to-bulk temperature difference in the pool.

$$-k \left.\frac{\partial T}{\partial z}\right|_{z=z_{max}-} = A\left(T\Big|_{z=z_{max}-} - T_{pool}\right)^{\beta} \qquad (3.1)$$

$$U_v\Big|_{z_{max}^-} = 0 \qquad (3.2)$$

A and $\beta$ are constants. The values in this paper are A=1840 $Wm^{-2}$ $K^{-1.35}$ and $\beta$ = 1.35. These are based on material in [4].

$T_{pool}$ is temperature of the overlying pool
(In this case a subcooled region at the top of the bed must exist).

3.1.2 Non-Subcooled pool

$$s = 1 \text{ at } z = z_{max} \qquad (3.3)$$

3.2 Bottom of Bed (at z = 0)

3.2.1 Conducting Impermeable bottom plate

The bed stands on a solid plate with thickness $z_p$, thermal conductivity $k_p$, specific heat capacity $c_p$, density $\rho_p$ and with internal heating rate $q_p$.

At the plate/bed interface

$$-k_p \frac{\partial T}{\partial z}\Big|_{z=0^-} = \Phi\Big|_{z=0^+} \qquad (3.4)$$

where

$$\Phi = \rho_v(c_v\ (T - T_{bp}) + h_v^o)\ U_v + \rho_\ell(c_\ell(T - T_{bp}) + h_\ell^o)U_\ell - k\frac{\partial T}{\partial z} \qquad (3.5)$$

and

$$0 = \rho_v U_v + \rho_\ell U_\ell \quad \text{at} \quad z = 0^+ \qquad (3.6)$$

This can be used to simplify (3.5)

$$\Phi = \rho_v c_v\ (T - T_{bp})U_v + \rho_\ell c_\ell(T - T_{bp})U_\ell + \rho_v U_v\ (h_v^o - h_\ell^o) - k\frac{\partial T}{\partial z}$$

which is an independent of the choice of $h_\ell^o$ as $h_v^o - h_\ell^o = L$.

In the plate

$$\rho_p c_p \frac{\partial T}{\partial t} = k_p \frac{\partial^2 T}{\partial z^2} \qquad (3.7)$$

At the bottom of the plate

$$T\Big|_{z=-z_p} = T_{plate} \tag{3.8}$$

where $T_{plate}$ is the temperature at the bottom of the plate which is specified as a boundary condition.

### 3.2.2 Adiabatic, Impermeable base

$$\Phi\Big|_{z=0+} = 0 \tag{3.9}$$

$$\rho_v U_v + \rho_\ell U_\ell = 0 \quad \text{at} \quad z=0+ \tag{3.10}$$

$$\Rightarrow \quad U_v = U_\ell = 0 \quad \text{at} \quad z = 0+ \quad \text{if} \quad T = T_{bp} \tag{3.11}$$

## 4. ENTHALPY FORMULATION

The model may be reformulated using an enthalpy function. This approach is used extensively in melting/freezing problems [5] where it can be used for numerical schemes which do not require the melt front to be tracked explicitly. In debris bed problems this approach also reduces the number of dependent variables from two (s and T) to one (enthalpy).

The enthalpy formulation in this paper differs from that used by Ruel and Mehr [6] in that it uses enthalpy per unit volume of bed rather than enthalpy per unit mass of liquid/vapour mixture. The approach of this paper has the advantage that there is a piecewise linear relationship between saturation and enthalpy as opposed to a non-linear relationship.

The enthalpy per unit volume h(s,T) defined by

$$\begin{aligned} h = \quad & (1-\varepsilon)\,\rho_d\,(c_d(T - T_{bp}) + h_d^0) && \text{- debris contribution} \\ & + \varepsilon s \rho_\ell\,(c_\ell(T - T_{bp}) + h_\ell^0) && \text{- liquid contribution} \\ & + \varepsilon(1-s)\,\rho_v\,(c_v\,(T - T_{bp}) + h_v^0) && \text{- vapour contribution} \end{aligned}$$

$$\text{with constraints } s=1, \text{ for } T<T_{bp}; \quad s=0, \text{ for } T>T_{bp} \tag{4.1}$$

The aim is to have s and T functions of h. This requires

$$\left.\frac{\partial h}{\partial s}\right|_{T=T_{bp}} < 0 \tag{4.2}$$

$$\Rightarrow \quad h_\ell^o < \frac{\rho_v L}{\rho_\ell - \rho_v} \tag{4.3}$$

$h_\ell^o = 0$ is generally used.

Figure 1 shows the enthalpy function h for two choices of $h_\ell^o$ : a) $h_\ell^o$ satisfies (4.3) so s and T are single valued functions of h. b) $h_\ell^o$ does not satisfy (4.3) so s and T are not single valued functions of h.

The continuity of heat flux, mass flux, saturation and temperature allows (2.2), (2.3) and (2.4) to be combined to give

$$\frac{\partial h}{\partial t} + \frac{\partial \Phi}{\partial z} = q \tag{4.4}$$

where

$$\Phi = \rho_v(c_v(T - T_{bp}) + h_v^o)\, U_v + \rho_\ell(c_\ell(T - T_{bp}) + h_\ell^o)\, U_\ell - k\frac{\partial T}{\partial z} \tag{4.5}$$

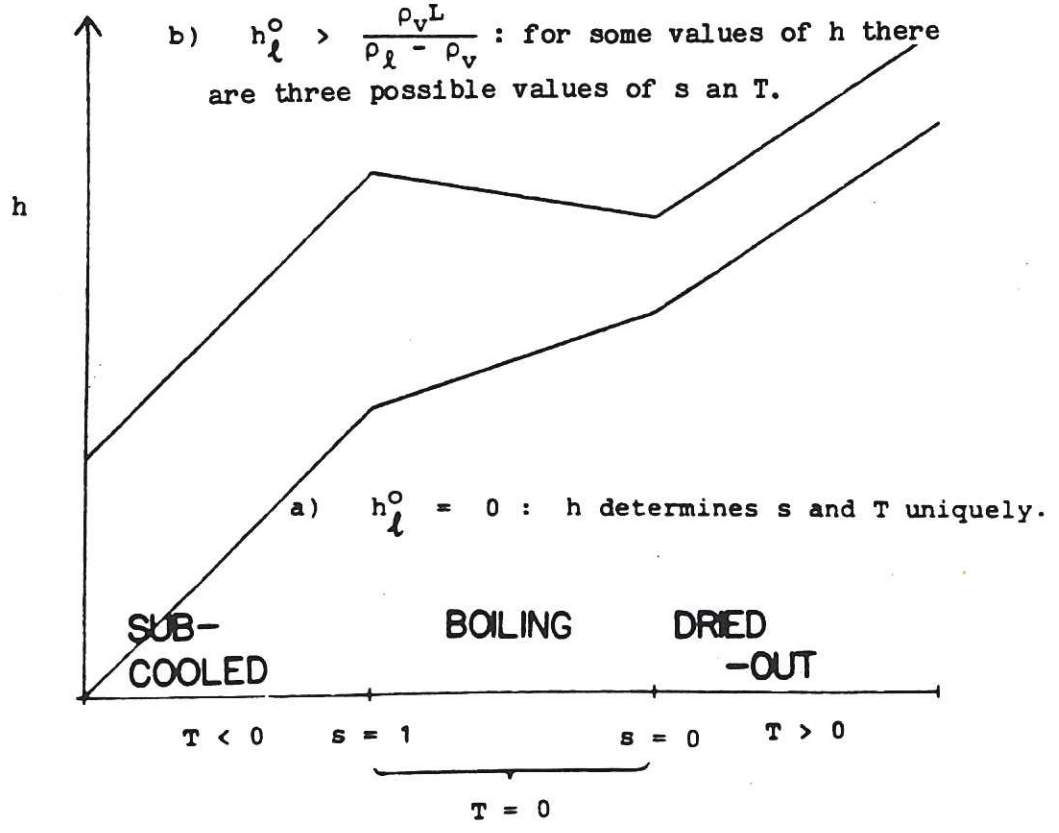


Fig. 1. Enthalpy function.

## 5. NUMERICAL SOLUTION

An explicit finite difference scheme is used. This has the advantage over implicit schemes that a complicated non linear solver is not required.

### 5.1 Spatial Mesh

A control volume approach is used on a staggered mesh. This leads to exact conservation of heat and mass in the numerical scheme. The bed is divided into N-1 cells of size $\Delta z$ with centre points at

$$z = (i - \frac{1}{2})\ \Delta z \quad (i=1,\ N-1) \tag{5.1}$$

where

$$\Delta z = z_{max}/(N-1) \tag{5.2}$$

h, s and T are discretized at the centre points of the cells

$$h_i = h(z=(i-\tfrac{1}{2})\Delta z) \tag{5.3}$$

$$s_i = s(h_i) \tag{5.4}$$

$$T_i = T(h_i) \tag{5.5}$$

Each cell is assumed to be either entirely subcooled, entirely boiling or entirely dried out. The cell is not allowed to change state during the timestep t to t + $\Delta t$ but may change state at the end of the step.

The superficial velocities are discretised according to

$$U_{vi} = U_v(z = i\Delta z) \tag{5.6}$$

$$U_{\ell i} = U_\ell(z = i\Delta z) \tag{5.7}$$

### 5.2 Discretisation of the Differential Equations

The equation for conservation of mass is discretised as

$$\varepsilon(\rho_\ell - \rho_v)\ \frac{s_i^n - s_i^o}{\Delta t} + \frac{\Phi_i^{mo} - \Phi_{i-1}^{mo}}{\Delta z} = 0 \tag{5.8}$$

where the mass flux

$$\Phi_i^m = \rho_v U_{vi} + \rho_\ell U_{\ell i}$$

superscripts o and n denote times t and t+$\Delta t$.

The enthalpy equation is discretised as

$$\frac{h_i^n - h_i^o}{\Delta t} + \frac{\Phi_i^o - \Phi_{i-1}^o}{\Delta z} = q \qquad (5.9)$$

where the enthalpy flux

$$\Phi_i^o = \rho_v(c_v(T_{vi}^o - T_{bp}) + h_v^o)U_{vi} + \rho_\ell(c_\ell(T_{\ell i}^o - T_{bp}) + h_\ell^o)U_{\ell i} - k_i^o\frac{(T_{i+1}^0 - T_i^0)}{\Delta z} \qquad (5.10)$$

where

$$k_i^o = k(\frac{1}{2}(s_i^o + s_{i+1}^o)) \qquad (5.11)$$

The choice of $T_{vi}^o$ and $T_{\ell i}^o$ is discussed later.

The dynamical equation becomes

in the boiling region,

$$\frac{\rho_v \nu_v U_{vi}^o}{K\,\phi_v(s_{vi}^o)}(1 + \frac{\alpha d\,|U_{vi}^o|}{(1-\varepsilon)\nu_v f_v}) - \frac{\rho_\ell \nu_\ell U_{\ell i}^o}{K\phi_\ell(s_{vi}^o)}(1 + \frac{\alpha d\,|U_{\ell i}|}{(1-\varepsilon)\,\nu_\ell f_\ell})$$

$$= (\rho_\ell - \rho_v)g - \sigma\cos\theta(\frac{\varepsilon}{K})^{1/2}(\frac{J(s_{i+1}^o) - J(s_i^o)}{\Delta z}, \qquad (5.12)$$

in the subcooled region,

$$U_{vi}^o = 0$$

and in the dried-out region

$$U_{\ell i}^o = 0\ .$$

## 5.3 Upwinding

It is preferable to use non-centred values for $T_{vi}$, $T_{\ell i}$, $s_{vi}$ and $s_{\ell i}$ in the evaluation of the mass and enthalpy fluxes.

In the single phase regions the usual upwinding for small conducted flux is

$$T_{vi} = \begin{cases} T_{i+1} & U_{vi} < 0 \\ T_i & U_{vi} \geq 0 \end{cases} \tag{5.13}$$

$$T_{\ell i} = \begin{cases} T_{i+1} & U_{\ell i} < 0 \\ T_i & U_{\ell i} \geq 0 \end{cases} \tag{5.14}$$

This upwinding is not necessary if the diffusion (heat conduction) is sufficiently large.

Upwinding in the flow equation (5.12) is also helpful. The upwinding

$$s_{vi} = \begin{cases} s_{i+1} & U_{vi} < 0 \\ s_i & U_{vi} \geq 0 \end{cases} \tag{5.15}$$

$$s_{\ell i} = \begin{cases} s_{i+1} & U_{\ell i} < 0 \\ s_i & U_{\ell i} \geq 0 \end{cases} \tag{5.16}$$

gives the most increase in mass diffusion (capillary pressure) and so should lead to the most stable numerical scheme in the boiling regions. However it is desirable to have $s_{vi}$ and $s_{\ell i}$ evaluated at the same point as otherwise both $\phi_v$ and $\phi_\ell$ could be zero in situations where $s_i = 1$ and $s_{i+1} = 0$. Therefore equations (5.15) and (5.16) are only used in cases with only boiling and dried-out regions and little capillary pressure. The recommended upwinding procedure is based on a 'wind'

$$\rho_v L U_v - k \frac{\partial T}{\partial z} \tag{5.17}$$

which may be overridden in the interior of single phase regions by (5.13) and (5.14).

There must be coherency between the upwinding of saturation and temperature to ensure that the equations can be solved to find $U_{vi}$ and $U_{\ell i}$. They must be evaluated at the same point at the boundaries i.e.

$T = T_{bp}$ when $0<s<1$

$T \neq T_{bp}$ when $s=0$ or $s=1$

Another consideration is that boiling regions must be allowed to grow and contract. The schemes suggested allow this.

## 5.4 Calculation Procedure

The basic dependent variable is the enthalpy h. Figure 2 shows the calculation procedure. $s_i^o$ and $T_i^o$ are calculated from $h_i^o$. $U_{vi}^o$ and $U_{\ell i}^o$ are then calculated by solving an 'elliptic' problem. The enthalpy is then updated using the enthalpy equation (5.9).

In the calculation of $U_{vi}^o$ and $U_{\ell i}^o$ from $s_i^o$ and $T_i^o$ the mass equation is used in the single phase region with either $U_{vi}^o=0$ or $U_{\ell i}^o=0$. This involves no time derivatives. In the boiling region the time derivatives are eliminated between (5.8) and (5.9) to produce

$$\frac{\Phi^{*o}_i - \Phi^{*o}_{i-1}}{\Delta z} = q \qquad (5.18)$$

where

$$\Phi^*_i = \Phi_i + \frac{\rho_v h_v^o - \rho_\ell h_\ell^o}{\rho_\ell - \rho_v} \Phi^m_i \qquad (5.19)$$

and the flow equation (5.12) is used to produce a set of algebraic equations.

Continuity of mass flux and heat flux are used at the boundaries between regions. Various boundary conditions are used. It is assumed that during the timestep t to t + $\Delta$t each cell remains in the same state as it was initially. At time t + $\Delta$t the cell is permitted to change state depending on the value of the enthalpy. This procedure produces a small truncation error when a cell does change state. However, the magnitude of the error can be estimated by checking the mass conservation which is exact elsewhere. These errors can be controlled by varying the cell size and the timestep and by choosing $h_\ell^o$ suitably.

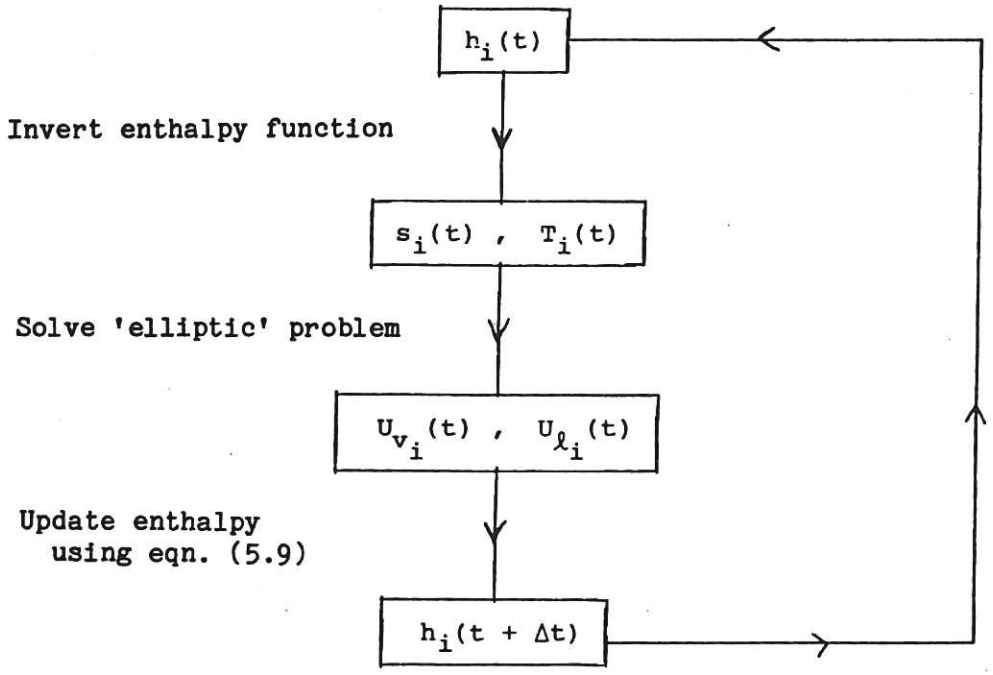


Fig. 2. Calculation procedure.

5.5 Numerical Treatment of Boundary Conditions

The top boundary conditions are treated as follows:

(3.1) becomes

$$\Phi^{o}_{N-1} = \rho_v(c_v(T_{N-1} - T_{bp}) + h^{o}_{v})\, U^{o}_{v\ N-1} + \rho_\ell(c_\ell(T_{N-1} - T_{bp}) + h^{o}_{\ell})\, U^{o}_{\ell_{N-1}} + A(1.5\, T_{N-1} - 0.5\, T_{N-2} - T_{pool})^{\beta} \qquad (5.20)$$

(3.2) becomes

$$U^{o}_{v\ N-1} = 0 \qquad (5.21)$$

(3.3) becomes

$$s_N = 1 \qquad (5.22)$$

(3.4) becomes

$$\Phi^{o}_{N-1} = \rho_v (c_v (T_{N-1} - T_{bp}) + h^{o}_{v})\, U^{o}_{v\,N-1} + \rho_\ell (c_\ell (T_{N-1} - T_{bp}) + h^{o}_{\ell})\, U^{o}_{\ell\,N-1} - \left(\frac{T_{bp} - T_{N-1}}{\Delta z}\right) \tag{5.23}$$

The bottom boundary conditions are treated in an analogous way. A standard explicit finite difference scheme is used in the bottom plate.

## 6. EXAMPLE CALCULATIONS

In these calculations the Leverett function proposed by Turland and Moore [7] has been used

$$J(s) = \begin{cases} 0.62 - 0.4s, & s < 0.8 \\ 14.7 - 53.2\, s + 66\, s^2 - \frac{55\, s^3}{2}, & s \geq 0.8 \end{cases} \tag{6.1}$$

The variation of J with s is illustrated in Figure 3.

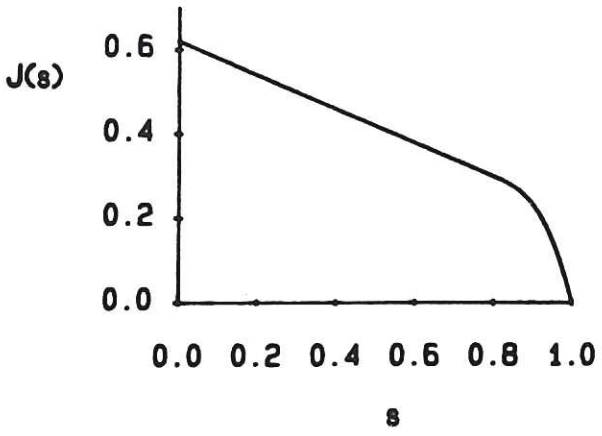


Fig. 3. Leverett function.

In addition, following Turland [8]

Cubic relative permeabilities

$$\phi_v(s) = (1-s)^3 \tag{6.2}$$

$$\phi_\ell(s) = s^3 \tag{6.3}$$

and linear turbulent enhancements

$$f_v(s) = 1-s \tag{6.4}$$

$$f_\ell(s) = s \tag{6.5}$$

are used in the flow equations and $\alpha$ is taken to be 0.01 which is consistent with the work of Burke and Plummer [9].
The permeability is calculated from the effective particle diameter and porosity using the Carmen-Kozeny formula:

$$K = \frac{d^2\varepsilon^3}{180\ (1-\varepsilon)^2} \tag{6.6}$$

The effective thermal conductivities of subcooled and dried-out regions are not known with any degree of accuracy. In the absence of any experimental measurements the Hashin and Shtrikman bounds [10] and Bruggeman formula [11] are used to guide the choice of an estimate. The Hashin Shtrikman bounds assume an isotropic and random mix of the constituents.

The lower/upper bound is given by

$$k = k_1 + \frac{A}{1 - A/3k_1} \tag{6.7}$$

$$A = \sum_{i \neq 1} \frac{\varepsilon_i}{\frac{1}{3k_1} + \frac{1}{k_i - k_1}} \tag{6.8}$$

where $k_1 = \min(k_i)$ gives the lower bound

$k_1 = \max(k_i)$ gives the upper bound

($k_i$ is the thermal conductivity of constituent i, $\varepsilon_i$ is its volume fraction).

The Bruggemann formula [11] which gives an estimate between these bounds is

$$\frac{1}{3k} = \sum_{i=1}^{n} \frac{\varepsilon_i}{k_i + 2k} \qquad (6.9)$$

Cook and Peckover [12] have suggested that as the Bruggeman formula does not distinguish between connected phases and unconnected phases then for real debris beds it can be used as an upper bound when the unconnected phase has the highest conductivity and as a lower bound when the connected phase has the highest conductivity.

## 6.1 Example 1: G1 test

This calculation is performed with the parameters appropriate to the second in-pile debris bed test in the MELUSINE reactor at Grenoble [13]. This test is now known as the G1 test [14]. In the 1-D model the bed is assumed to be 0.2 m deep, supported on a 0.02 m steel plate and with an overlying sodium pool. The overlying pool is assumed to be at a fixed temperature of 400°C. The temperature of the bottom of the supporting plate is also fixed at 400°C. A sodium coolant at 2 bar is used. The effective debris particle diameter is .255mm (including shape factor). The debris consists of 80% $UO_2$ and 20% stainless steel by weight. The porosity of the bed is 0.35.

Calculations have been performed for the following case. The bed starts in a steady state with no internal heating (the bed is fully saturated with liquid and at a uniform temperature of 400°C. The power in the bed is then increased to 3 $MW/m^3$ in a single step and held constant.

To guide the choice of an effective thermal conductivity for sub-cooled regions, the Hashin Shtrikman bounds and Bruggeman formula are evaluated using properties at 800°C

$$k_{min}^{HS} = 10.4 \text{ W m}^{-1} \text{ K}^{-1}$$

$$k_{max}^{HS} = 20.4 \text{ W m}^{-1} \text{ K}^{-1}$$

and the Bruggeman estimate is

$$k^B = 16.0 \text{ W m}^{-1} \text{ K}^{-1} .$$

In the calculation $k_{sat} = 18 \text{ W m}^{-1} \text{ K}^{-1}$ is used.

To guide the choice of an effective thermal conductivity for dried-out regions, the Hashin Shtrikman bounds and Bruggeman formula are evaluated using properties at the saturation temperature (964°C)

$$k^{HS}_{min} = 0.420 \text{ W m}^{-1} \text{ K}^{-1}$$

$$k^{HS}_{max} = 4.32 \text{ W m}^{-1} \text{ K}^{-1}$$

$$k^B = 2.36 \text{ W m}^{-1} \text{ K}^{-1}.$$

In the calculation $k_{dry} = 1.4 \text{ W m}^{-1} \text{ K}^{-1}$ is used.

The numerical scheme required k(s) for all s in the range 0 to 1.

$k(s) = sk_{sat} + (1-s)k_{dry}$ is used.

The upwinding is described by (5.13), (5.14) for T and the wind (5.17) is used for s.

Twenty mesh points are used in the bed with one mesh point in the bottom plate. This makes the cells in the plate and bed roughly the same size. (N.B. the thermal conductivity of the plate is roughly the same as that of the liquid filled bed.)

Figure 4 shows how the saturation and temperature profiles vary with time.

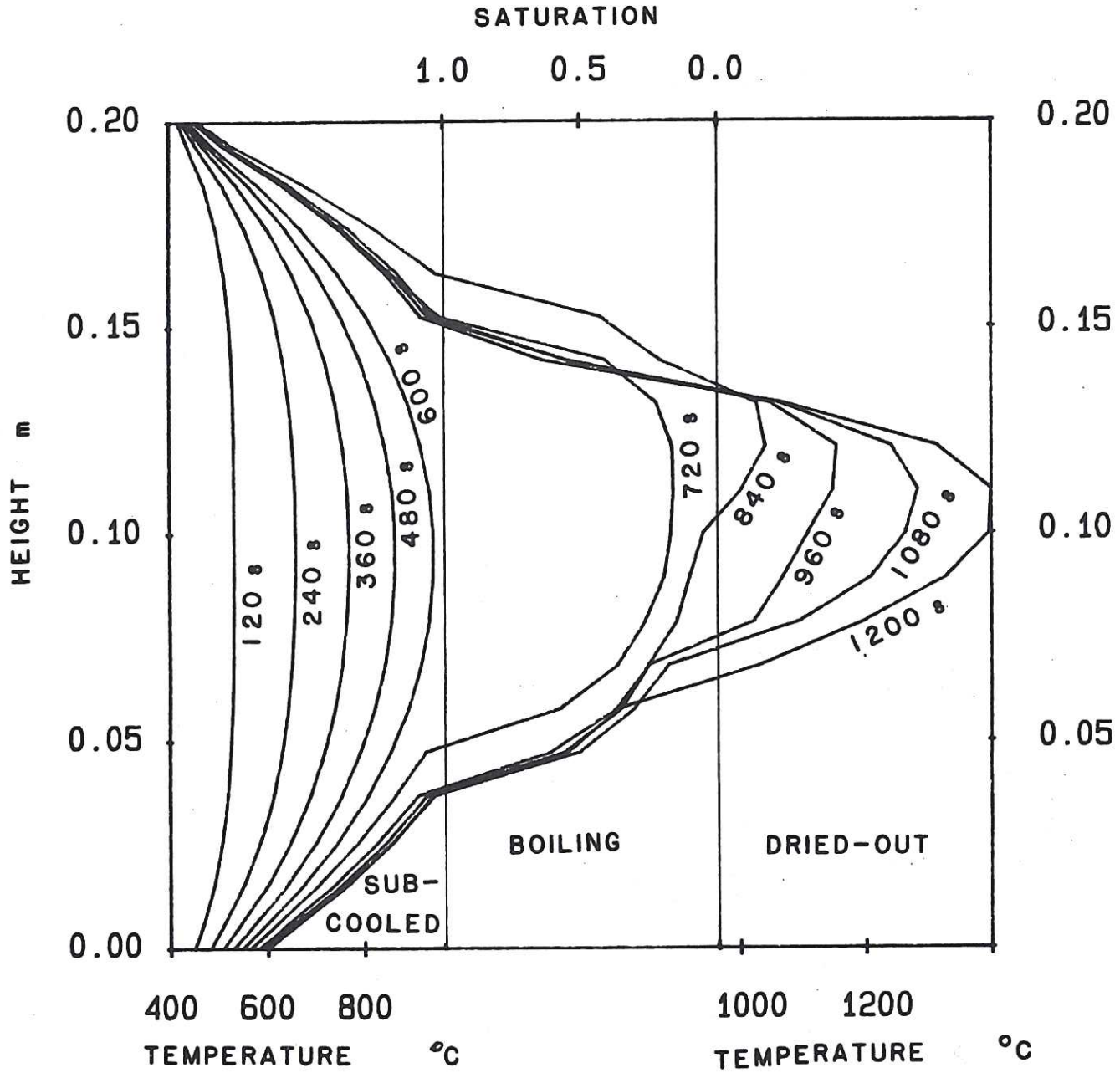


Fig. 4. Transient calculation for G1 test. Power stepped up to 3 MW/m$^3$ from zero in bed at uniform temperature of 400° C. Results shown at 120 second intervals.

## 6.2 Example 2: DCC2 test

This example uses data appropriate to the DCC2 experiment performed at Sandia [15]. The debris consists of $UO_2$ particles with effective diameter 1.42 mm (including shape factor) in a 0.5 m high bed with an adiabatic, impermeable base and a non-subcooled overlying pool. The porosity of the bed is 0.384.

For this calculation the water coolant is assumed to be under pressure with a saturation temperature of 160°C (approx. 6.2 bar pressure). Calculations have been performed for the following transient. The bed starts in a steady state for a reactor power of 255 kW. The power is stepped up to 625 kW for 400s and then stepped up to 990 kW for a further 450s after which it is switched off.

Bed power q, is assumed to be related to reactor power Q through [16]

$$\frac{q}{Q} = A\rho_d\,(1-\varepsilon)\,(0.5866 + 4.939z - 9.878z^2) \times (1 + .81s)$$

where $A = 0.53 \times 10^{-3}\ kg^{-1}\ m^{-3}$

To guide the choice of an effective thermal conductivity for the dried-out region, the Hashin Shtrikman bounds and Bruggeman formula are evaluated using water properties at 160°C and a $UO_2$ conductivity of 3.5 W $m^{-1}$ $K^{-1}$.

$$k^{HS}_{min} = 0.172\ W\ m^{-1}\ K^{-1}$$

$$k^{HS}_{max} = 1.827\ W\ m^{-1}\ K^{-1}$$

$$k_B = 1.52\ W\ m^{-1}\ K^{-1}$$

The value $k_{dry} = 0.4$ W $m^{-1}$ $K^{-1}$ is used in the calculation.
$k(s) = k_{dry}$ is used in the numerical scheme.

The upwinding is based on (5.13), (5.14), (5.15) and (5.16). Thirty mesh points are used in the calculation.

Figure 5 shows how the saturation and temperature profiles vary with time. After 850s, when the power is switched off, quenching of the debris occurs. The quench is complete in approximately 500 seconds.

Figure 6 shows the behaviour when the quench front reaches the impermeable, adiabatic base of the bed. When this occurs the heat flux into the base of the boiling region suddenly drops to zero and consequently the vapour flux at the base also drops to zero.

The timescale over which the change from a 'S' shape profile to a flat profile occurs is of order 15 s. This short time is partially due to the (unphysical) idealized boundary condition. More detailed modelling of the DCC-2 capsule would lead to a prediction of longer times.

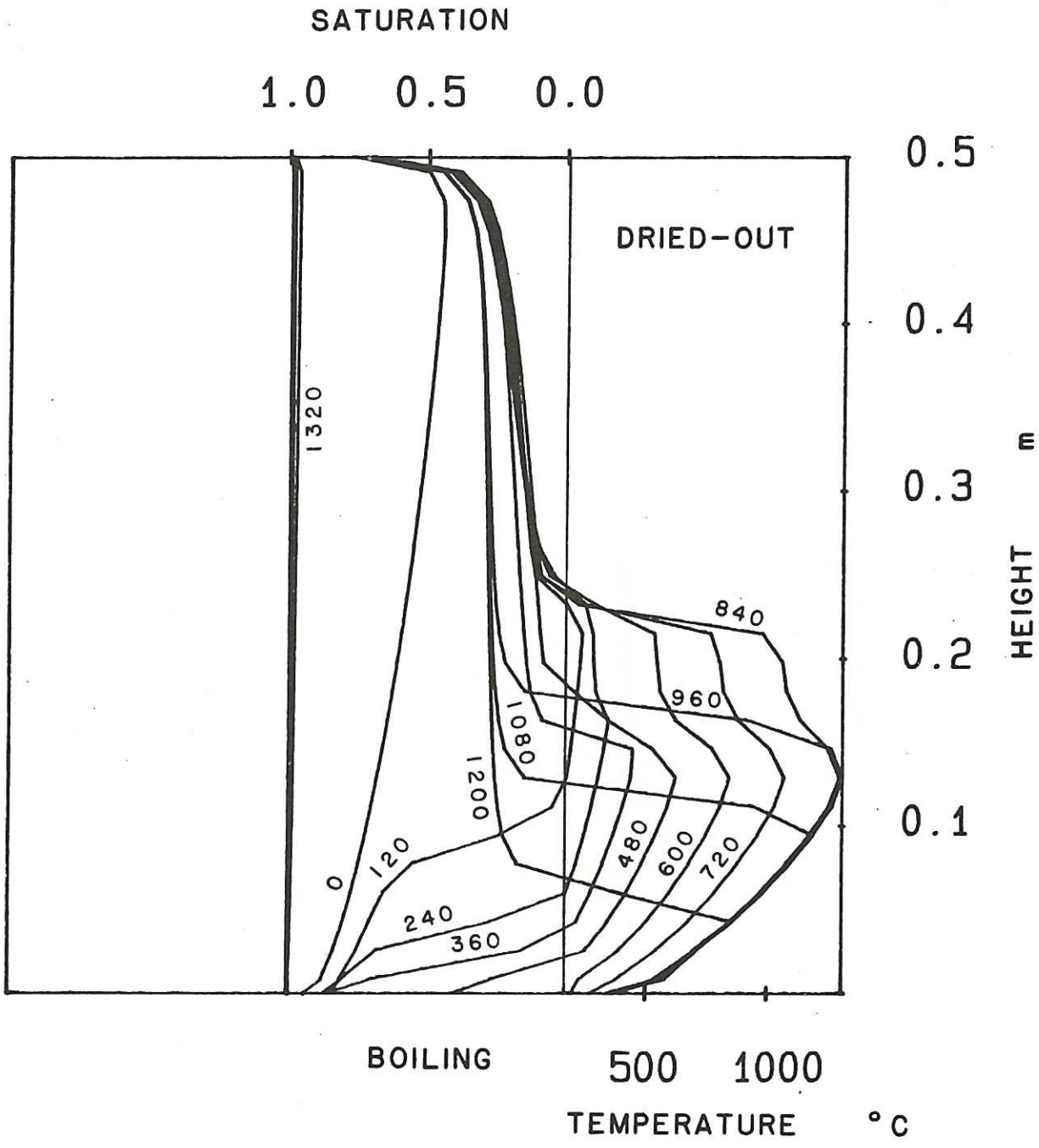


Fig. 5. Transient calculation for DCC-2 test. Power steps at 0 s and 400 s. Power switched off at 850 s. Results shown at 120 second intervals.

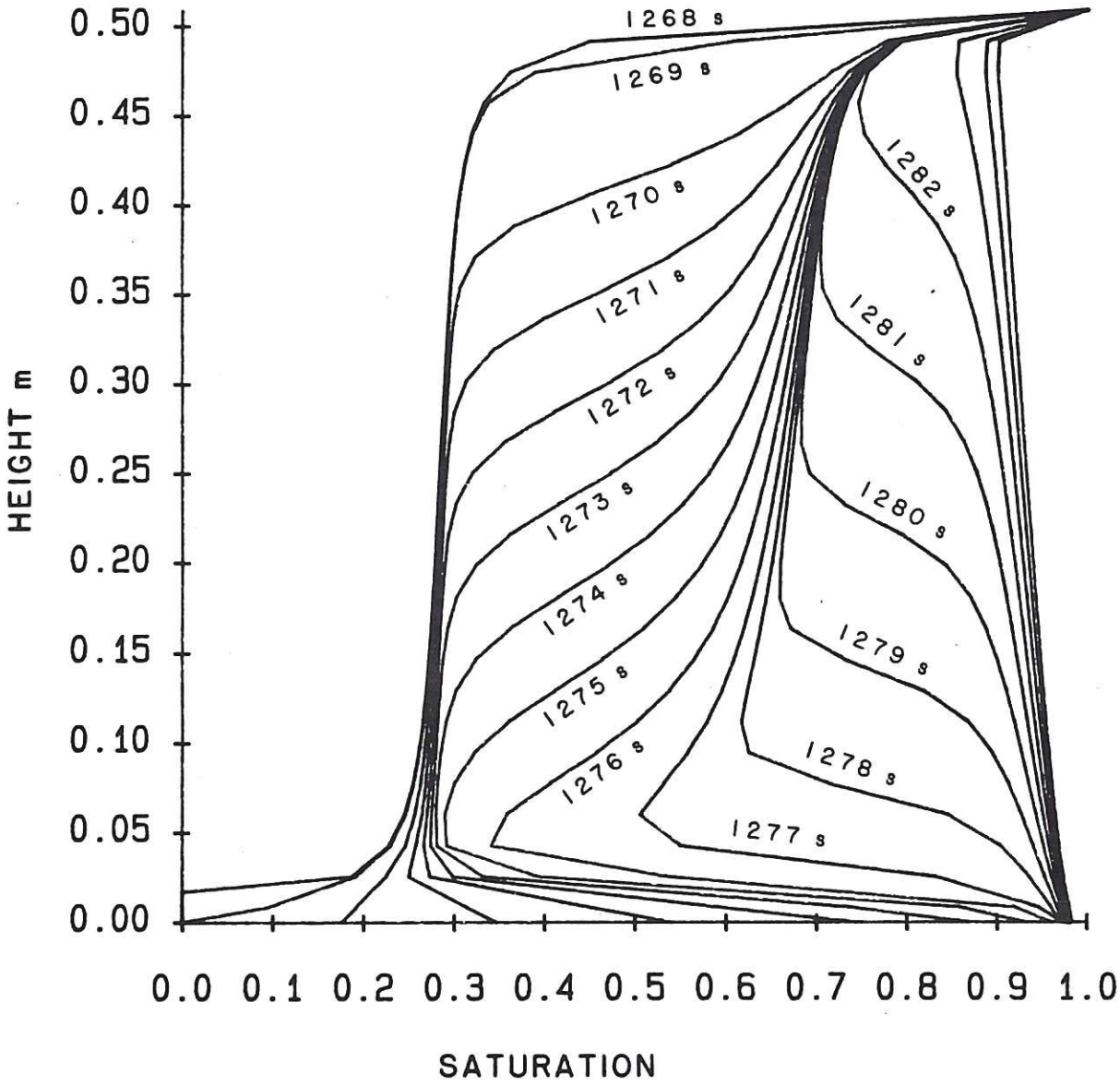


Fig. 6. Expansion of figure 5 when quench front reaches base. Saturation profile displayed at 1 second intervals.

## 7 MODEL LIMITATIONS

### 7.1 Temperature dependence

The assumption was made that the bed and coolant properties did not vary with temperature. This assumption is not necessary and inclusion of the temperature dependence of these properties would require little programming effort due to the explicit nature of the scheme. However, the expense in terms of function evaluations in the code would be high as the explicit scheme needs a large number of relatively small timesteps.

Typically, k and $\rho_v$ may vary by a factor of two or more and $c_v$, $c_\ell$, $c_d$ and $\rho_c$ may have variations of up to 20% over the temperature range in a typical calculation. The variation in $\rho_d$ can be neglected. Other properties are only required at the saturation temperature which does not vary much (see next section). The temperature dependence of k will affect the maximum temperature in the dried-out region. The variation in $\rho_v$ will tend to increase vapour flow rates.

### 7.2 Pressure dependence

It was also assumed that physical properties did not vary with pressure. This inclusion of pressure dependence would be a more difficult task. It would require an enthalpy function dependent on pressure:

$h(s, T, p_v)$ in boiling/dried out regions

or $h(s, T, p_\ell)$ in boiling/subcooled regions

$p_v$ or $p_\ell$ could be calculated from (2.5) or (2.6) at each step.

The pressure variation is greatest when capillary pressure is large. In general the effect is small and will cause a small variation in the local saturation temperature which will give rise to a small conducted heat flux through boiling regions.

### 7.3 Steel melting

The model described in this paper is no longer valid if the temperature in a dried-out zone rises to the steel melting temperature. The model could easily be extended a little by including the latent heat of melting of stainless steel (through a jump in the enthalpy h). However, the treatment of steel migration would be a very difficult task.

## 7.4 Bed disruptions and channelling

When large power steps occur in the bed the generation of vapour may cause the debris to be displaced. After this disruption has occurred properties of the bed such as the porosity and permeability may be changed. A condition which may be used to determine when and where a disruption occurs is

$$P_\ell(z) - P_\ell(z_{max}) > (1-\varepsilon)\,\rho_d g\,(z_{max} - z) \qquad (7.1)$$

i.e. when the upward force on the debris from liquid exceeds the weight of debris.

However, the pressures derived from the theory of this paper are macroscopic averages and the detail of the flows around the particles are not known: therefore this condition has not been incorporated in the present model.

Channelling occurs when debris is displaced to form channels through which vapour can flow with less restriction than through the debris. Conditions for when channelling occurs and modified flow equations for the channelled region need to be developed before this phenomenon can be included in the model.

## 7.5 Hysteresis in capillary pressure

The model described in this paper uses the same Leverett Function (capillary pressures) for drainage and imbibition whereas, experimentally, different Leverett functions are found. It would be possible to select different Leverett functions depending on the history of the bed. However, there would be complications as the drainage Leverett function and the imbibition function are just bounds and not the only possible ones. It would also be difficult to decouple the numerical treatment from the choice of functions used.

# 8 CONCLUSION

Calculations for the time dependent behaviour of 1-D debris beds in which sub-cooled, boiling and dried-out regions are present can now be

performed. This is a significant aid to model development and validation as it allows transient data from experiments to be compared with model predictions. It is recommended that more comparisons between the model and experiments are made before further improvements to the code are made.

## 9 ACKNOWLEDGEMENTS

The author thanks Dr. B.D. Turland and Dr. Katharine Moore for many useful discussions.

## 10 REFERENCES


1. Lipinski R J. A Model for Boiling and Dryout in Particle Beds. Sandia Laboratory Report SAND82 - 0765 (NUREG/CR - 2146) (1982).

2. Turland B D and K A Moore. Debris Bed Heat Transfer with Top and Bottom Cooling. 21st ASME/AIChE Heat Transfer Conference, Seattle, 25-28 July, 1983, and published in AIChE Symposium Series, No.225, Vol.79, pp.250-255, 1983.

3. Turland B D and Katharine Moore. One Dimensional Models of Boiling and Dryout. Post Accident Debris Cooling, Müller U and Günther C (Eds), G Braun, Karlsruhe (1982).

4. Joly C and C le Rigoleur. General and particular aspects of the particulate bed behaviour in the PAHR situation for LMFBRs. Fluid dynamics of porous media in energy applications, Von Karman Institute lecture series notes (1979).

5. Atthey D R. A finite difference scheme for melting problems based on the method of weak solutions. Moving Boundary Problems in heat flow and diffusion (J R Ockendon and W R Hodgkins, eds.) p.182-191.

6. Fuel F and Mehr K. A numerical model of boiling and dry-out in particle beds for the analysis of the European in-pile tests. 11th Meeting of the LMBWG, October 23-26, 1984. Grenoble - France.

7. Stevens G F. Particle-bed Heat Transfer Studies at AEE Winfrith. Presented at the first UK national heat transfer conference, Leeds (July 1984).

8. Turland B D ed. Compendium of Post Accident Heat Removal Models for Liquid Metal Cooled Fast Breeder Reactors. Study contract ECI 959-B 7221-82UK, Final report (Oct 1983).

9. As reported in Bird R B, Stewart W E and Lightfoot E N. Transport Phenomena, John Wiley and Sons, New York, p.199 (1960).

10. Hashin Z and Shtrikman S. A Variational Approach to the Theory of Effective Magnetic Permeability of Multiphase Materials. J. Appl. Phys. Vol. 33, pp. 3125-3131, (1962).

11. Bruggeman D A G. Dielectic Constant and Conductivity of Mixtures of Isotropic Materials. Ann. Phys., Vol 24, p 636 (1935).

12. Cook I and Peckover R S. Effective Thermal Conductivity of Debris Beds. ibid 3 pp 40-45.

13. Rousseau D, Veyrat J F and Holtbecker H. The In-Pile PAHR Experiments in MELUSINE Reactor. ibid 3 pp 215-220.

14. Simoni O. Private Communication. October 1984.

15. Reed A W, Bergeron E D, Boldt K R and Schmidt T R. Coolability of $UO_2$ Debris Beds in Pressurized Water pools: DCC-1 and DCC-2 Experiment Results. Proceedings of Sixth Information Exchange Meeting on Debris Coolability. Los Angeles, November 1984.

16. Reed A W. Private Communication.

*Available from*
HER MAJESTY'S STATIONERY OFFICE
49 High Holborn, London, WC1V 6HB
*(Personal callers only)*
P.O. Box 276, London, SE1 9NH
*(Trade orders by post)*
13a Castle Street, Edinburgh, EH2 3AR
41 The Hayes, Cardiff, CF1 1JW
Princess Street, Manchester, M60 8AS
Southey House, Wine Street, Bristol, BS1 2BQ
258 Broad Street, Birmingham, B1 2HE
80 Chichester Street, Belfast, BT1 4JY

PRINTED IN ENGLAND